Bandgap engineering of electronic and optoelectronic devices on native AlN and GaN substrates: a modelling insight

V. F. Mymrin [a], K. A. Bulashevich [a,b], N. I. Podolskaya [a], S. Yu. Karpov [a,c],

[a] *Soft-Impact, Ltd., P.O.Box 83, 27 Engels av., St.Petersburg, 194156 Russia*

[b] *Ioffe Physico-Technical Institute RAS, 26 Polytechnicheskaya, St.Petersburg, 194021 Russia*

[c] *Semiconductor Technology Research, Inc., P.O.Box 70604, Richmond, VA, 23255-0604, USA*

Abstract

Native GaN and AlN substrates cut out of single-crystal boules provide threading dislocations in on-grown III-nitride materials with the density much lower than that observed in structures on conventional sapphire or SiC wafers. The native substrates are also expected to enable an easy choice of growth surface orientation that controls the crystal polarity and, hence, the distribution of polarization charges in a nitride heterostructure. The impact of these factors on the bandgap engineering of advanced electronic and optoelectronic devices is discussed in this paper in terms of numerical simulation with the focus on high-electron mobility transistors and light-emitting diodes.

Preprint (2005)

Key words:
B1. Nitrides, B3. Field effect transistors, B3. Light emitting diodes
PACS: 81.05.Ea, 85.60.Bt, 85.30.Tv, 85.60.Jb

1. Introduction

Group-III nitride optoelectronic and electronic devices have been fabricated for a decade, using commercial sapphire and SiC substrates. Cheap sapphire substrates are found to be quite suitable for a large-scale production of planar low-power blue/green light-emitting diodes (LEDs), while relatively expensive SiC substrates are used for fabrication of compact vertical low-power and high-power LEDs [1,2]. In addition, SiC substrates are currently indispensable for making high-power field-effect transistors (FETs), which is due to the extremely high thermal conductivity of SiC necessary for a proper thermal management of the devices [3].

Today, however, disadvantages of sapphire and SiC substrates have become quite evident. First, a large mismatch between the lattice constants and the thermal expansion coefficients of the substrates and nitride epitaxial materials [2] produces a high threading dislocation density, $\sim 10^8 - 10^{10}$ cm^{-2}, in device heterostructures grown by metalorganic vapor phase epitaxy (MOVPE) or molecular beam epitaxy (MBE). On the one hand, threading dis-

* Corresponding author.
Email address: karpov@semitech.us (S. Yu. Karpov).

locations induce an intensive non-radiative carrier recombination in optoelectronic devices, LEDs and laser diodes (LDs), resulting in a low internal quantum efficiency [4–6]. On the other hand, the high dislocation density leads to an enhanced degradation of both optoelectronic and electronic devices, especially under high-current operation conditions [7]. Second, the large difference between the refractive indices of sapphire (1.75) and nitride semiconductors ($\sim$ 2.3 in GaN, $\sim$ 2.15 in AlN, and $\sim$ 2.9 in InN [8]) is the origin of light waveguiding in a heterostructure on a sapphire substrate, which lowers the efficiency of light extraction from the LED. The waveguiding effect is negligible in LED structures grown on SiC substrates. However, SiC substrates are transparent only to visible light, making their application in ultra-violet (UV) LEDs problematic. The problems of light extraction are so critical that they have initiated the development of special technologies of substrate removal after the growth of LED structures, aimed at increasing the overall LED efficiency [9,10]. In the case of FETs, the high dislocation density in nitride materials grown on silicon, sapphire, or SiC substrates reduces the device reliability and lifetime, initiates premature breakdown, and leads to a greater noise [11].

A natural solution to the above problems is to employ native GaN and AlN substrates. The substrate materials are complimentary rather than competitive. Being readily doped with silicon, GaN substrates are quite suitable for fabricating high-power LEDs and LDs operating in the visible and UV spectral ranges [12–14]. It has been demonstrated that the dislocation density in nitride heterostructures on bulk GaN substrates does not exceed $\sim 10^4$ cm^{-2} [15], which should resolve the problems of non-radiative carrier recombination and a rapid degradation of optoelectronic devices. In the case of UV LEDs, especially of those operating at 250-300 nm, AlN substrates seem to be more advantageous due to (i) their potential transparency to emitted light and (ii) a lower (compressive) strain in the epilayers grown on these substrates (for comparison, AlGaN layers on GaN exhibit a tensile strain, frequently resulting in their cracking). Having a high thermal conductivity, $\sim$ 70% of that of SiC, and a high intrinsic resistance, AlN is apparently the best substrate material for high-power FETs. In addition, a dislocation density of $\sim 10^5$ cm^{-2} demonstrated in the FET structure on a native AlN wafer [11] has allowed a considerable reduction in the leakage current.

Presently, commercial GaN and AlN substrates are not available. This is because of the lack of growth technologies suitable for industrial production of AlN and GaN bulk crystals. Much progress has been made in the development of growth techniques in recent years. In particular, sublimation growth of AlN bulk crystals of 20 mm long and 15 mm in diameter was demonstrated in [16]. AlN wafers cut out of these crystals exhibited a dislocation density less than $\sim 10^3$ cm^{-2} and a high crystalline quality confirmed by X-ray difractometry [17]. These substrates were successfully used for the fabrication of UV LEDs [18] and high-electron mobility transistors (HEMTs) [11].

At the moment, the high-pressure crystal growth from the solution remains the only reliable technique providing bulk GaN crystals of sufficient size [19]. However, to use this method for a large-scale production, we should resolve the problems associated with the low growth rate and poorly controlled crystal shape [20]. So, alternative approaches have been developed, using quasi-bulk materials (boules and thick epitaxial layers with reduced dislocation density) grown by hydride vapor phase epitaxy (HVPE). Two-inch GaN wafers with a dislocation density less than $\sim 10^4$ cm^{-2} obtained by this technique have been demonstrated in [21]. Besides, quasi-bulk GaN templates with a dislocation density in the range of $2-5\times10^7$ cm^{-2} are available commercially [22]. Recently, the HVPE technique has been applied to grow quasi-bulk AlN [23]. These achievements in the fabrication of GaN and AlN wafers has provided their ever broadening use in technology of advanced wide-bandgap semiconductor devices.

A specific feature of III-nitride heterostructures is a strong piezoeffect and spontaneous electric polarization producing huge polarization charges accumulated primarily at the interfaces [26]. Polarization charges may negatively or positively affect the device characteristics, depending on the device structure. In addition to a low-dislocation density, a proper cutting of substrates from bulk AlN and GaN would enable easy control of the

growth surface orientation for epitaxy of nitride heterostructures. In analogy with conventional III-V compounds, this seems to be much easier than the use, for instance, of conventional non-polar substrates, as the latter normally results in a high density of dislocations ($\sim 10^{10}$ cm^{-2}) and stacking faults ($\sim 10^5$ cm^{-1}) for materials grown on both sapphire and SiC substrates [24,25]. The polarity control through the choice of native substrate orientation opens new opportunities for designing device heterostructures, which have not been discussed in literature.

This paper is aimed at a better understanding of a possible impact of native substrates on bandgap engineering of III-nitride devices. We have simulated a specific charge distribution in HEMT heterostructures on AlN and have examined strain effects on sheet electron concentration in the channel. The role of a structure polarity in the carrier confinement in visible and UV LEDs and the threading dislocation effect on the internal quantum efficiency of the devices is evaluated by modelling. The theoretical predictions are compared with available observations.

2. Modeling

The simulation of HEMTs was based on a self-consistent solution of the coupled Poisson and Schrodinger equations for both electrons and holes, which accounted for possible two-dimensional hole gas (2DHG) in some III-nitride heterostructures. The complex valence band structure of nitride semiconductors was allowed for within the approach of Ref.[27]. The Fermi-Dirac statistics was used to consider high carrier concentrations in the electron and hole channels.

To simulate the LED operation, we used the SiLENSe package [28] implementing a 1D-model based on the Poisson equation for the electric potential and the drift-diffusion transport equations for the electron and hole concentrations. The bimolecular radiative recombination of the carriers and their non-radiative recombination on threading dislocation cores [6] were considered to predict the internal quantum efficiency of an LED. Light emission spectra were found from the Schrödinger equations for the electron and hole wave functions. A uniform spectral broadening was assumed in the spectrum computations.

We accounted for the specific properties of nitride semiconductors, like a strong piezoeffect, the spontaneous electric polarization, a low efficiency of acceptor activation, and a high threading dislocation density typical to epitaxial materials. The numerical models employed were capable of analyzing graded-composition layers providing both a built-in pulling field and a distributed polarization doping [29].

3. HEMTs on AlN substrate

Generally, a HEMT on an AlN substrate forms a double-heterostructure (DHS) with a narrow-bandgap GaN channel between a wide-bandgap AlN substrate (or an AlN buffer layer) and an AlGaN cap layer. If the DHS is grown in the [0001] direction, which corresponds to an Al-faced growth surface, a large negative polarization charge arises at the GaN/AlN interface, and a smaller positive charge is accumulated at the AlGaN/GaN interface. The latter favors two-dimensional electron gas (2DEG) formation at the AlGaN/GaN interface, irrespective of whether the AlGaN cap is doped with donors or not.

Our simulation of a HEMT heterostructure coherently grown on an AlN(0001) substrate, similar to that reported in [11], shows that in addition to the 2DEG formed at the AlGaN/GaN interface, a 2DHG is induced at the negatively charged GaN/AlN interface, as discussed in [11]. This effect is quite general and should occur in most DHS transistors.

If the GaN layer is thick enough, the 2DHG avoids the shunting of the 2DEG by background electrons in the structure bulk. In this case, however, the main advantage of DHS, namely, the suppression of electron spillover by the electric field built-in in the GaN channel, cannot be utilized in full measure, because the field vanishes with the channel thickness. A reduction in the channel thickness improves the electron confinement,

Refer to: J. Cryst. Growth **281**, No.1, 115-124 (2005)/**DOI** 10.1016/j.jcrysgro.2005.03.019

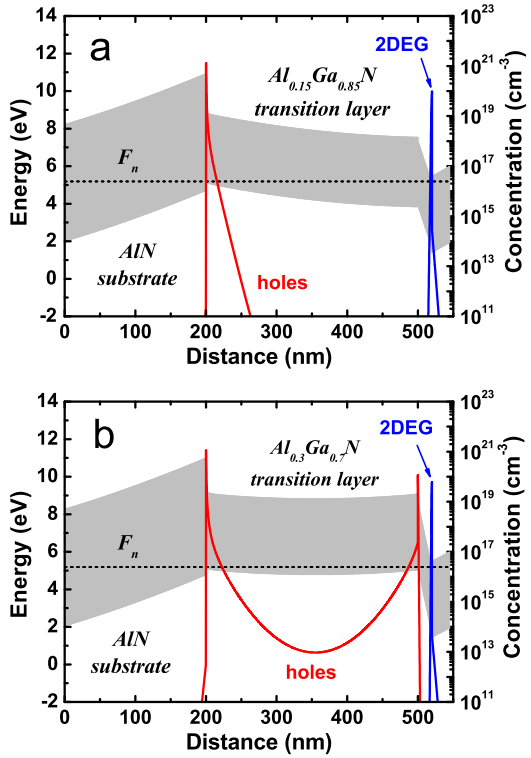

Fig. 1. Equilibrium band diagrams and carrier concentrations in unintentionally doped HEMT structures with $Al_{0.15}Ga_{0.85}N$ (a) and $Al_{0.3}Ga_{0.7}N$ (b) transition layers [31]. The Schottky barrier height is 0.8 V, according to [31]. Bandgap is marked by shadow.

preventing the electron spillover towards the bulk. Nevertheless, the co-existence of the 2DEG and 2DHG in a thin GaN channel may affect negatively the HEMT performance. Indeed, the ohmic source and drain contact regions formed by annealing may overlap both the 2DEG and 2DHG channels. This is expected to result in shunting the electron conductivity by the parasitic holes. In addition, the electrons heated in the electric field induced by the drain-source voltage are capable of penetrating into the 2DHG region, leading to carrier losses through the electron-hole recombination. Finally, the existence of the 2DHG at the GaN/AlN interface makes the application of the back-doping concept [30] problematic.

The parasitic holes cannot be easily compensated for by simply doping the underlying AlN layer, as this requires thick layers with an extremely high donor concentration N_D, which is hard to grow because of technological reasons. Even the doping of 1 μm AlN with $N_D = 5 \times 10^{19}$ cm^{-3} is found to be still insufficient for a complete suppression of the 2DHG.

To improve the electron confinement in the GaN channel, a special $Al_xGa_{1-x}N$ transition layer has been suggested to be inserted between the SiC substrate and the channel [31]. We have tested this approach by modelling such a HEMT structure on an AlN substrate. It turns out that the parasitic holes disappear from the bottom GaN/AlGaN interface, if the AlN fraction x in the transition layer does not exceed 0.15 (Fig.1a). This is due to redistribution of polarization charges in the heterostructure and their screening by background electrons. At $x \geq 0.3$, however, the holes generated by polarization charges fill up the transition layer, approaching the 2DEG channel (see Fig.1b). This result is in agreement with estimates made in [31].

Our simulations also predict the sheet electron concentration to be less than $\sim 5 \times 10^{12}$ cm^{-2} in a HEMT heterostructure with an $Al_{0.15}Ga_{0.85}N$ transition layer. This value is lower than the concentration of $\sim 7 - 12 \times 10^{12}$ cm^{-2} normally observed in an conventional AlGaN/GaN single heterostructure (SHS). The reason for the reduction in the sheet concentration in a DHS on AlN is a compressive strain produced by the lattice mismatch. This strain induces a negative charge at the GaN-channel/AlGaN-cap interface via piezoeffect, which compensates partly for a positive charge due to spontaneous polarization. As the result, the total charge at the interface is lower than in the SHS exhibiting a tensile strain, leading to a reduced sheet electron concentration in the DHS.

An alternative way of avoiding a parasitic hole channel invokes a coupled profiling of the composition and donor concentration in the $Al_xGa_{1-x}N$ transition layer (see Fig.2a). It includes both conventional and distributed-polarization doping in a graded-composition layer [29], which provides an additional degree of freedom for the HEMT structure design. The coupled composition and doping profiling allows a complete elimination of parasitic holes (Fig.2b), which is predicted to hold at a widely ranged gate bias.

As mentioned above, DHS HEMTs on AlN ex-

Refer to: J. Cryst. Growth **281**, No.1, 115-124 (2005)/**DOI** 10.1016/j.jcrysgro.2005.03.019

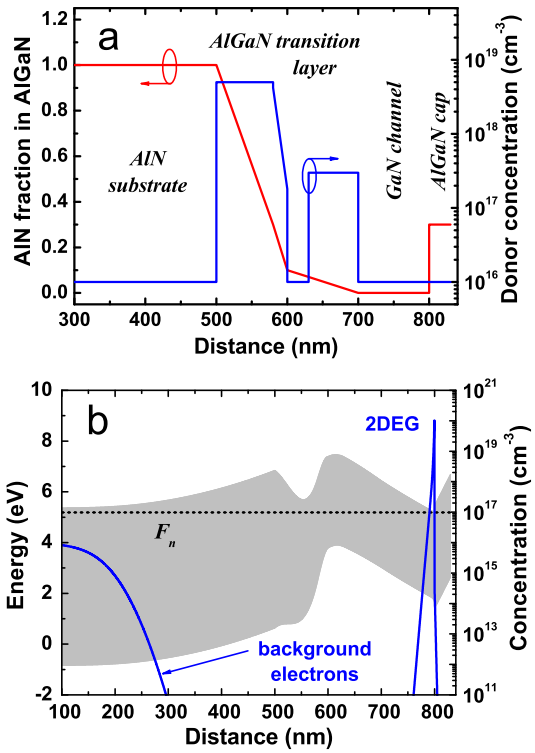

Fig. 2. Dopant concentration and composition profiles (a), the equilibrium band diagram and the electron concentration (b) of a HEMT structure on AlN(0001) substrate. The Schottky barrier height of 1.2 V is taken in the simulations. Bandgap is marked by shadow.

hibit a sheet carrier concentration lower than that in the conventional AlGaN/GaN HEMTs. This disadvantage can be overcome by using AlN-rich AlGaN caps owing to a compressive strain preventing their cracking. Indeed, the cap cracking limits the AlGaN composition in SHS HEMTs by a value of $x \sim 0.3 - 0.35$ at a cap thickness of $\sim 25 - 20$ nm [32]. Actually, this cuts down the sheet electron concentration to $\sim 2 \times 10^{13}$ cm^{-2} [33]. In the DHS HEMTs, the 2DEG concentration can be effectively controlled by choosing a proper cap. Our simulations show that the sheet concentration of $0.5 - 1.5 \times 10^{13}$ cm^{-2} can be readily obtained by varying the cap design from 30 nm $Al_{0.3}Ga_{0.7}N$ to 2nm AlN/6 nm $Al_{0.3}Ga_{0.7}N$. As the maximum of the 2D-electron mobility is reported to be observed at $0.8 - 1.5 \times 10^{13}$ cm^{-2} [34–36], the variation in the sheet concentration provided by different caps is sufficient to attain high-performance DHS HEMTs on AlN substrates.

4. LEDs on native nitride substrates

In this section we discuss two aspects of using native GaN and AlN substrates to fabricate III-nitride LEDs. One is the influence of the substrate orientation on polarization charges at the interfaces and, hence, on the LED characteristics. The other is the effect of threading dislocation density on the LED internal quantum efficiency (IQE), i.e. the ratio of the photon emission rate per unit area to the flux of electrons/holes crossing the structure.

4.1. *Substrate orientation effect on LED operation*

Substrates cut out of bulk AlN and GaN crystals would allow an easy control of the growth surface orientation with respect to the hexagonal axis of nitride materials, which is the key factor determining the polarization charges at the interfaces. To understand the role of crystal polarity in LED operation, we compare the characteristics of the same AlGaN/InGaN/GaN single-quantum-well (SQW) heterostructure (see [37] for details) assumed it to be grown on a Ga-faced, an N-faced, or a non-polar substrate.

Fig.3 shows the band diagrams of these LEDs computed for nearly the same density of current through the devices. It is seen that in the Ga-faced structure, there is a barrier hindering the electron injection into the SQW active region. A similar but slightly lower barrier is also formed in the non-polar LED structure but no remarkable barrier is observed in the N-faced one. The latter is due to a positive polarization charge at the InGaN/GaN interface, considerably narrowing the space-charge region in n-GaN. Moreover, there is an excellent confinement of both electrons and holes in the N-faced structure due to the p-AlGaN and n-GaN barriers preventing the minority carrier penetration into the p- and n-regions, respectively. It is this factor that increases the IQE of the N-faced heterostructure, especially pronounced at low current densities (Fig.4).

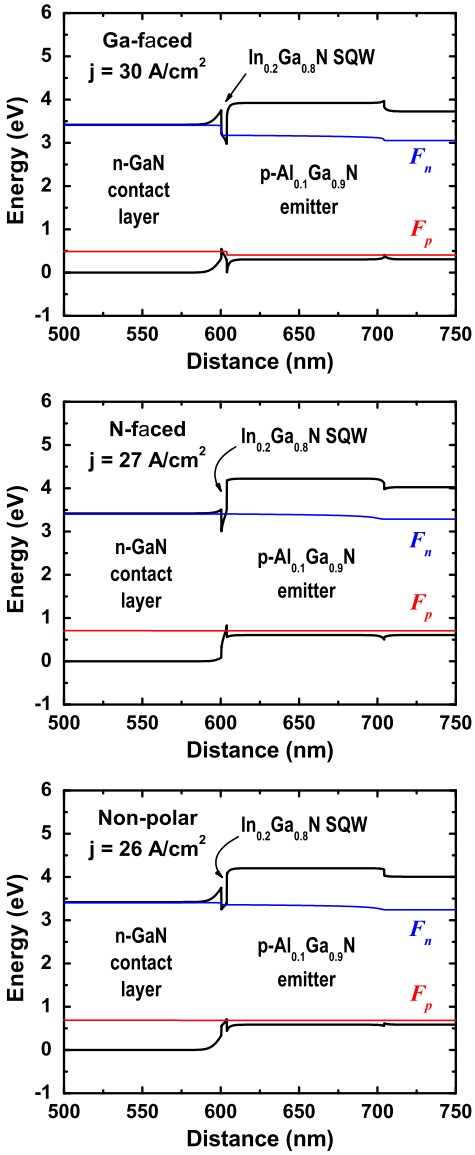

Fig. 3. Band diagrams of a blue SQW AlGaN/InGaN/GaN LED on Ga-faced, N-faced, and non-polar substrates at the bias of 3.0, 2.7, and 2.72 V, respectively.

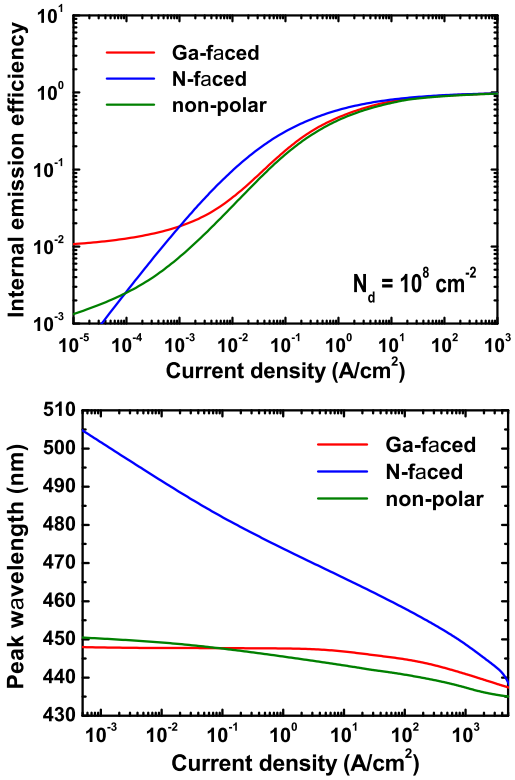

Fig. 4. IQE (top) and peak emission wavelength as a function of current density computed for the LED structures on substrates of different orientations.

It is quite surprising that the non-polar LED structure exhibits a slightly lower IQE than the Ga-polar one (see Fig.4), in contrast to natural expectations. The point is that the negative charge at the InGaN/GaN interface enhances the barrier hindering the carrier injection into the SQW. However, the same charge attracts holes that come from the p-AlGaN emitter, increasing the hole concentrations by a factor of 1.5-2.0, as compared with the non-polar SQW. This eventually rases the IQE of the Ga-faced LED. Keeping in mind that the overlap of electron and hole wave functions has not been considered rigorously in the radiative recombination model above, one should take this quantitative result with some caution. Further efforts are necessary to conclude whether a non-polar structure is inferior to a Ga-faced one.

Fig.4 also demonstrates the behavior of the peak emission wavelength *versus* the current density computed for the above heterostructures. It is seen that the Ga-faced LED provides the highest wavelength stability in the practical range of current density variation, $10^{-1} - 10^{2}$ A/cm^2. This is due to the fact that the p-n junction electric field is opposite to the electric field induced by the polarization charges at the SQW interfaces.

Therefore, the bias or, the current density variation, results in a smaller change of the quantum well profile with bias and, eventually, in a better wavelength stability. The poorest spectrum stability is predicted for the N-faced heterostructure, where the external and built-in polarization fields are unidirectional. On the other hand, the shift of the peak wavelength with current in the N-faced LED can be employed for tuning the color of the emitted light from cyan (at a low current density) to blue (at a high current density).

4.2. *LED internal quantum efficiency*

An amazing property of III-nitride semiconductors, which was immediately exploited in practice, is a relatively high IQE of blue InGaN LED structures grown on conventional sapphire or SiC substrates, observed in spite of an extremely high threading dislocation density in epitaxial materials. On the basis of numerous studies, this observation has been attributed to the InGaN composition fluctuations in quantum wells, accumulating non-equilibrium carriers in the local In-rich regions far from dislocations (see, e.g, [7,38]). However, at high current densities typical of high-power LED and LD operation, the non-equilibrium carriers fill up not only the In-rich regions but also the rest of the quantum well, reducing the IQE. In UV LEDs with In-free epitaxial layers, the dislocation effect on the IQE is a more critical factor limiting the total efficiency of the device [4,5,14]. Thus, the use of low-dislocation substrates becomes vital to the improvement of device performance. Here this issue is considered with reference to UV LED heterostructures.

Recently, a UV LED emitting at 290 nm with a record output power of $\sim$ 1.35 mW has been demonstrated at the Sandia Labs [39]. Two types of LED chip, with a rectangular 200×200 μm^2 contact geometry and 1×1 mm^2 interdigitated contacts, were examined in [39]. Using simulation, we have found a correlation between the IQE of the LED theoretically predicted for the threading dislocation density $N_d = 10^{10}$ cm^{-2} and the external emission efficiency measured in a wide range of current density (see Fig.5). The low-current discrepancy seen for both types of device is apparently associated with a non-radiative recombination channel other than the dislocation-mediated one. The discrepancy observed at high currents in the rectangular LED may be attributed to the structure heating. Both factors were neglected in simulations. The predicted IQE can be compared quantitatively with the measured external efficiency, assuming the light extraction yield to be $\sim 2\%$.

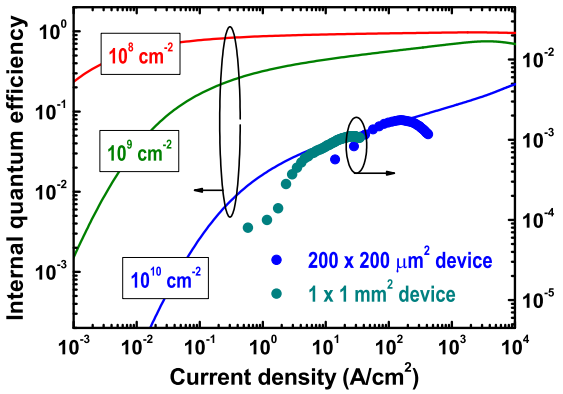

Fig. 5. IQE *versus* current density computed for the UV LED structure from Ref.[39]. Circles are external LED efficiency measured in [39] for different device types . Numbers in frames indicate the corresponding threading dislocation densities.

The simulations show that at $N_d = 10^{10}$ cm^{-2}, the IQE varies in the range of 2-7% with the current density increasing from 1 to 100 A/cm^2. Reduction in the threading dislocation density to 10^9 cm^{-2} increases the IQE approximately by an order of magnitude. Further reduction in N_d to 10^8 cm^{-2} allows one to attain an IQE no longer limited by the non-radiative carrier recombination on threading dislocations.

The dramatic rise in the IQE due to dislocation density reduction allows the implementation of thick active regions in In-free LED heterostructures. Indeed, in conventional LEDs, the InGaN active region cannot be made thick enough because of strain relaxation via generation of misfit dislocations and V-defects negatively affecting the IQE. In In-free LEDs, much thicker active regions can be utilized, which mitigates technological requirements on interface quality, as compared to quantum-well LED heterostructures. On the other

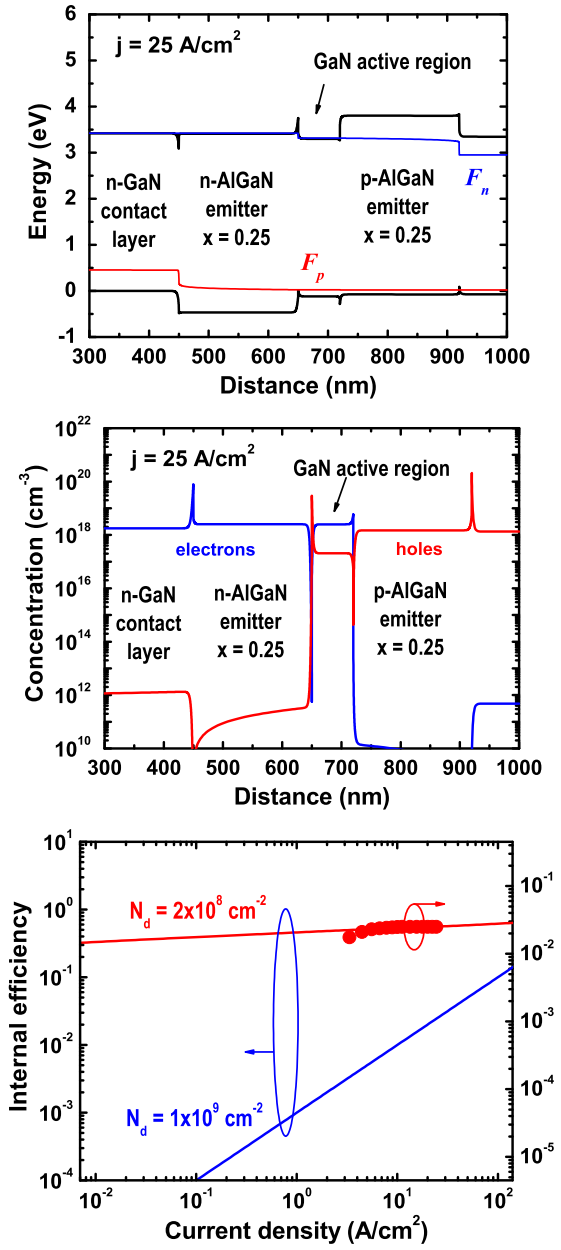

Fig. 6. Band diagram and distributions of carrier concentrations at the bias of 3.4 V, and IQE as a function of current density computed for the AlGaN/GaN/AlGaN violet LED structure from Ref.[41]. Circles indicate the external efficiency measured at different currents.

hand, the non-equilibrium carrier concentrations in a thick active region are normally lower than those in a quantum-well one. As the IQE rises with the carrier concentration [6], the use of a thick active region requires a reduced threading dislocation density.

To date, there have been a few examples of successful use of thick active regions in violet and UV LEDs [40,41]. In [40], the low dislocation density of $\sim 2 \times 10^7$ cm^{-2} was achieved by the lateral overgrowth of an AlGaN buffer layer on an artificial saw-tooth template. In [41], the dislocation density was controlled by adjusting the thickness of a HVPE-grown GaN buffer. The latter approach allowed a reduction of N_d from 1×10^9 cm^{-2} to 2×10^8 cm^{-2}.

Fig.6 shows the band diagram and carrier concentrations in the AlGaN/GaN/AlGaN violet LED structure of [41] computed for the operating current density of 25 A/cm^2. One can see that electrons and holes are well confined by AlGaN emitters in the thick GaN active region. The IQE predicted for $N_d = 2 \times 10^8$ cm^{-2} is weakly dependent on the current density, which fits well the measured external efficiency (Fig.6). In contrast, the IQE computed for $N_d = 1 \times 10^9$ cm^{-2} is found to increase remarkably with the current density. The computations also indicate that the IQE up to $\sim$ 50% can be obtained at $N_d = 2 \times 10^8$ cm^{-2} in an LED structure with a thick active region (this estimate accounts only for the non-radiative recombination on threading dislocations). At $N_d = 1 \times 10^9$ cm^{-2}, the IQE is predicted to be about by an order of magnitude lower, which agrees with the electro-luminescence data reported in [41]. The reduction in the dislocation density below $2 - 5 \times 10^7$ cm^{-2} enables a complete elimination of the dislocation effect on the IQE.

5. Conclusion

We have employed simulation to analyze some specific features of bandgap engineering of advanced III-nitride semiconductor devices, HEMTs and LEDs, on native AlN and GaN substrates. The low-dislocation density in materials grown on such substrates and the potentially easy control of crystal polarity by cutting out the wafers of a

desired orientation from a boule opens new ways for improvement of the device performance.

HEMTs fabricated on AlN substrates generally form a DHS with co-existing electron and hole gases. We have examined a number of approaches to avoid negative effects of the parasitic holes on the characteristics of HEMTs with a thin GaN channel. Among them, there is an approach based on a coupled profiling of the composition and doping in a transition layer between the AlN substrate and the GaN channel. This procedure is shown to eliminate completely the parasitic holes in a wide range of bias values. Additionally, the sheet electron concentration in such a structure can be effectively controlled by a proper design of the AlGaN cap layer, providing the concentrations corresponding to the maximum mobility of 2DEG in the GaN channel. Compressive strain in a HEMT structure on AlN prevents the AlGaN cap cracking, which allows exploiting caps with a high AlN content.

An essential contribution of the crystal polarity to the LED operation is demonstrated with reference to a blue SQW heterostructure. An N-faced LED is shown to provide a better carrier confinement near the SQW active region, as compared to Ga-faced or non-polar structures. No remarkable difference in the carrier injection efficiency has been found for the Ga-faced and non-polar LEDs. A better emission wavelength stability is predicted in the Ga-faced LED due to a specific interplay between the p-n junction electric field and the polarization field in the SQW. In contrast, the peak wavelength in an N-faced LED structure shifts considerably with current through the device.

A dramatic effect of threading dislocation density on the IQE is shown with reference to In-free UV and violet LEDs. The found correlation between the theoretically predicted IQE and the measured external emission efficiency supports the idea of a dominant role of the dislocation-mediated non-radiative carrier recombination. For the LED structures considered in the paper, a reduction in the dislocation density below $\sim 10^7$ cm^{-2} eliminates nearly completely the dislocation effect on the IQE. The use of native GaN and AlN substrates to provide low-dislocation epitaxial heterostructures allows the use of rather thick active regions, which are easy to fabricate in In-free LEDs. This approach commonly utilized in red AlGaAsP LEDs provides additional degrees of freedom for bandgap engineering of high-power UV LEDs.

Acknowledgment. The authors thank Prof. Alexander Zhmakin of the Joint Supercomputing Centre (St.Petersburg, Russia) for helpful discussion of the results. The work of K. A. Bulashevich is supported in part by the Russian Federal Program on Support of Leading Scientific Schools, grant 2160.2003.2.

References

[1] O. Ambacher, J. Phys. D **31** (1998) 2653.

[2] L. Liu and J. H. Edgar, Mat. Sci. Engineer. R **37** (2002) 61.

[3] S. J. Pearton, F. Ren, A. P. Zhang, and K. P. Lee, Mat. Sci. Engineer. R **30** (2000) 55.

[4] T. Hino, S. Tomiya, T. Miyajima, K. Yanashima, S. Hashimoto, and M. Ikeda, Appl. Phys. Lett. **76** (2000) 3421.

[5] M. Iwaya, S. Terao, T. Sano, S. Takanami, T. Ukai, R. Nakamura, S. Kamiyama, H. Amano, and I. Akasaki, Phys. Status Solidi (a) **188** (2001) 117.

[6] S. Yu. Karpov and Yu. N. Makarov, Appl. Phys. Lett. **81** (2002) 4721.

[7] S. Nakamura, J. Cryst. Growth **201/202** (1999) 290.

[8] V. Bougrov, M. Levinshtein, S. Rumyantsev, and A. Zubrilov, in: M. E. Levinshtein, S. L. Rumyantsev, and M. S. Shur, eds. *Properties of Advanced Semiconductor Materials: GaN, AlN, InN, BN, SiC, SiGe* (John Wiley and Sons, Inc., New York, 2001), Ch.1.

[9] T. Fujii, Y. Gao, R. Sharma, E. L. Hu, S. P. DenBaars, and S. Nakamura, Appl. Phys. Lett. **84** (2004) 855.

[10] T. Frey and V. Härle, *Abstract Book of the 14th International Conference on Crystal Growth* (2004) 431.

[11] X. Hu, J. Deng, N. Pala, R. Gaska, M. S. Shur, C. Q. Chen, J. Yang, G. Simin, M. Asif Khan, J. C. Rojo, and L. J. Schowalter, J. Cryst. Growth **82** (2003) 1299.

[12] T. Mukai, S. Hagahama, T. Yanamoto, and M. Sano, Phys. Stat. Solidi (a) **192** (2002) 261.

[13] P. Perlin, P. Wiśniewski, T. Swietlik, L. Gorczyca, M. Leszczyński, T. Suski, P. Prystawko, R. Czernecki, K. Krowicki, I. Grzegory, and S. Porowski, *Abstract Book of the 3rd International Workshop on Bulk Nitride semiconductors* (2004) 59.

[14] K. Akita, T. Nakamura, and H. Hirayama, Phys. Stat. Solidi (a) **201** (2004) 2624.

[15] A. Gassmann, T. Suski, N. Newman, C. Kisielowski, E. Jones, E. R. Weber, Z. Liliental-Weber, M. D. Rubin, H. I. Helava, I. Grzegory, M. Bockowski, J. Jun, and S. Porowski, J. Appl. Phys. **80** (1996) 2195.

[16] J. C. Rojo, G. A. Slack, K. Morgan, B. Raghothamachar, M. Dudley, and L. J. Schowalter, J. Cryst. Growth. **231** (2001) 317.

[17] B. Raghothamachar, M. Dudley, J. C. Rojo, K. Morgan, and L. J. Schowalter, J. Cryst. Growth **250** (2003) 244.

[18] http://optics.org/articles/news/8/4/27/1#uvled

[19] S. Porowski, J. Cryst. Growth **189/190** (1998) 153.

[20] I. Grzegory, M. Bockowski, B. Lucznik, S. Krukowski, Z. Romanowski, M. Wroblewski, and S. Porowski, J. Cryst. Growth **246** (2002) 177.

[21] R. P. Vaudo, X. Xu, C. Loria, A. D. Salant, J. S. Flynn, and G. R. Brandes, Phys. Stat. Solidi (a) **194** (2002) 494.

[22] http://www.lumilog.com ; http://www.tdii.com

[23] Yu. Melnik, V.Soukhoveev, V. Ivantsov, V. Sizov, A. Pechnikov, K. Tsvetkov, O. Kovalenkov, V. Dmitriev, A. Nikolaev, N. Kuznetsov, E. Silveira, and J. Freitas, Jr. Phys. Sta. Solidi (a) **200** (2003) 22.

[24] M. D. Craven, S. H. Lim, F. Wu, J. S. Speck, and S. P. DenBaars, Appl. Phys. Lett. **81** (2002) 469.

[25] M. D. Craven, F. Wu, A. Chakraborty, B. Imer, U. K. Mishra, S. P. DenBaars, and J. S. Speck, Appl. Phys. Lett. **84** (2003) 1281.

[26] F. Bernardini, V. Fiorentini, and D. Vanderbilt, Phys. Rev. B **63** (2001) 193201.

[27] S.-H. Park and S.-L. Chuang, J. Appl. Phys. **87** (2000) 353.

[28] http://www.semitech.us/products/SiLENSe/

[29] D. Jena, S. Heikman, J. S. Speck, U. K. Mishra, A. Link, and O. Ambacher, Phys, Stat. Solidi (c) **0** (2003) 2339.

[30] N. Maeda, K. Tsubaki, T. Saitoh, and N. Kobayashi, Mat. Res. Soc. Symp. Proc. **693**(2002) I12.8.1.

[31] C. Q. Chen, J. P. Zhang, V. Adivarahan, A. Koudymov, H. Fatima, G. Simin, J. Yang, and M. Asif Khan, Appl. Phys. Lett. **82** (2003) 4593.

[32] Z. Bougrioua, I. Moerman, L. Nistor, B. Van Daele, E. Monroy, T. Palacios, F. Calle, and M. Leroux, Phys. Stat. Solidi (a) **195** (2003) 93.

[33] O. Ambacher, J. Smart, J. R. Shealy, N. G. Weimann, K. Chu, M. Murphy, W. J. Schaff, L. F. Eastman, R. Dimitrov, L. Wittmer, M. Stutzmann, W. Reager, and J. Hilsenbeck, J. Appl. Phys. **85** (1999) 3222.

[34] R. Oberhuber, G. Zandler, and P. Vogl, Appl. Phys. Lett., **73** (1998) 818.

[35] C. Q. Chen, J. P. Zhang, V. Adivarahan, A. Koudymov, H. Fatima, G. Simin, J. Yang, and M. Asif Khan, Appl. Phys. Lett. **82** (2003) 4593.

[36] S. R. Kurtz, A. A. Allerman, D. D. Koleske, A. G. Baca, and R. D. Briggs, J. Appl. Phys, **95** (2004) 1888.

[37] S. Yu. Karpov, K. A. Bulashevich, I. A. Zhmakin, M. O. Nestoklon, V. F. Mymrin, and Yu. N. Makarov, Phys. Stat. Solidi (b) **241** (2004) 2668.

[38] B. Monemar, J. P. Bergman, J. Dalfors, G. Pozina, B. E. Sernelius, P.O. Holtz, H. Amano, and I. Akasaki, MRS J. Nitride Semicond. Res. **4** (1999) 16.

[39] A. J. Fischer, A. A. Allerman, M. H. Crawford, K. H. A. Bogart, S. R. Lee, R. J. Kaplar, W. W. Chow, S. R. Kurtz, K. W. Fullmer, and J. J. Figiel, Appl. Phys. Lett. **84** (2004) 3394.

[40] M. Iwaya, S. Takanami, A. Miyazaki, Y. Watanabe, S. Kamiyama, H. Amano, and I. Akasaki, Jpn. J. Appl.Phys. **42** (2003) 400.

[41] A. S. Usikov, D. V. Tsvetkov, M. A. Mastro, A. I. Pechnikov, V. A. Soukhoveev, Y. V. Shapovalova, O. V. Kovalenkov, G. H. Gainer, S. Yu. Karpov, V. A. Dmitriev, B. OMeara, S. A. Gurevich, E. M. Arakcheeva, A. L. Zakhgeim, and H. Helava, Phys. Stat. Solidi (c) **0** (2003) 2265.